Available online at www.sciencedirect.com

ScienceDirect

Solar Energy 132 (2016) 143–149

SOLAR ENERGY

www.elsevier.com/locate/solener

Investigation of parasitic absorption and charge carrier recombination losses in plasmonic silicon solar cells using quantum efficiency and impedance spectroscopy

Eshwar Thouti, Vamsi K. Komarala *

Centre for Energy Studies, Indian Institute of Technology Delhi, New Delhi 110016, India

Received 10 November 2015; received in revised form 23 February 2016; accepted 1 March 2016
Available online 19 March 2016

Communicated by: Associate Editor Frank A. Nüesch

Abstract

Quantum efficiency and impedance spectroscopy tools are employed for understanding the influence of parasitic absorption losses and partial field effect surface passivation by the silver nanoparticles (Ag NPs) on electrical properties of textured silicon solar cells without and with Si_3N_4 spacer layer. The parasitic absorption losses from Ag NPs reduced the internal quantum efficiency near the surface plasmon resonance region. The passive components like; series and parallel resistances, chemical capacitance of solar cells without and with Ag NPs are estimated after fitting impedance semicircles, which are further used for estimating effective carrier lifetime (τ_{eff}) values. Under AM1.5G illumination, cells with Si_3N_4 spacer layer showed a large decrease in the τ_{eff} due to the strong parasitic absorption losses from the Ag NPs. But, the cells without Si_3N_4 spacer layer showed a small decrease in the τ_{eff} due to the reduced surface recombination after partial field effect passivation from near-fields of Ag NPs' surface plasmon resonances on the emitter surface.

Keywords: Silicon solar cell; Silver nanoparticles; Impedance spectroscopy; Effective carrier lifetime; Parasitic absorption

1. Introduction

Recently, metal nanoparticles (NPs) are considered as an alternate for confining light/enhancing optical absorption in various types of solar cells with the excitation of localized surface plasmon resonances (SPRs). In the literature, much has been reported about optical properties of metal NPs for light trapping in solar cells. A few configurations are proposed for integrating metal NPs in cell structure; placing directly on front surface, embedding in active medium, and also integrating at rear side of cell structure (Atwater and Polman, 2010). For silicon based cells, researchers have employed metal NPs, mainly either on front or rear surface (Pillai et al., 2007; Beck et al., 2009; Tan et al., 2012; Spinelli et al., 2012; Pudasaini and Arturo, 2013; Manisha et al., 2014a,b). When the metal NPs are integrated at rear side of silicon cell for light trapping, minimal plasmonic related losses like; interband transitions and parasitic absorption losses are observed (Beck et al., 2009; Atwater and Polman, 2010; Tan et al., 2012; Manisha et al., 2014a,b). When metal NPs integrated on front surface of silicon cell, the detrimental factors (parasitic absorption) associated with NPs are overshadowed the beneficial effects (Beck et al., 2009; Pudasaini and Arturo, 2013; Thouti et al., 2014; Das et al., 2015), which curtailed the light trapping efficiency in the silicon. Apart

* Corresponding author.
E-mail addresses: eshwariitd@gmail.com (E. Thouti), vamsi@ces.iitd.ac.in (V.K. Komarala).

http://dx.doi.org/10.1016/j.solener.2016.03.002
0038-092X/

from the parasitic absorption losses from metal NPs (Spinelli and Polman, 2012), other loss mechanism related to modified carrier surface recombination process at silicon surface-NPs interface without/with a thin spacer layer has been overlooked (Yang et al., 2012; Barugkin et al., 2013; Tong et al., 2014; Thouti et al., 2014).

There is no such experimental study, which can distinguish the parasitic absorption losses and modified charge carrier recombination at the interface due to the metal NPs. Since, these two mechanisms have strong influence on any opto-electronic device performance after integrating the metal NPs (Thouti et al., 2014; Sero et al., 2009), so, there is a need to understand the individual loss mechanism on device performance. For understanding the optical and/or electronic losses of plasmonic cells, conventional DC characterization techniques such as current–voltage and quantum efficiency measurements are routinely employed. Some basic studies of plasmonic silicon cells related to incident wavelength dependent photocurrent reduction in SPR region, and modification of minority carrier diffusion lengths in off-resonance region of metal NPs are reported recently (Thouti et al., 2014).

The aim of this work is to understand plasmonic silicon cells' performance modification after integration of silver (Ag) NPs due to the parasitic absorption losses and partial field effect passivation at the cell emitter-Ag NPs interface. We made an attempt to segregate these two mechanisms by investigating effective carrier lifetime (τ_{eff}) values of Ag NPs integrated textured silicon cells without and with Si_3N_4 spacer (anti-reflection) layer using quantum efficiency and impedance spectroscopy (IS) techniques. The AC frequency analysis of plasmonic cell can help for quantifying passive components like; recombination resistance and junction capacitance; these parameters are further used for estimating of τ_{eff} (Sero et al., 2009; Kumar et al., 2014). Since, these passive components of device are sensitive to any variation in the physical structure, which can provide some microscopic insights related to the cell emitter-metal NPs interface.

2. Experimental procedure

The textured silicon solar cells without and with Si_3N_4 layer of thickness ~75 nm were used in this study, which are obtained from different sources. The Si_3N_4 thin film acts as surface passivation layer as well as anti reflection coating (ARC) on cells, and the fabrication procedure of these cells is similar to the details reported elsewhere (Thouti et al., 2014). Before the Ag NPs preparation on the cell front surface, cells were pre-annealed at 300 °C for 1 h in nitrogen ambient to avoid any temperature dependent modifications during experimentation in device structure, these cells are called in the discussion as C0 (cells without ARC) and ARC0 (cells with ARC). The Ag NPs were prepared from thermally evaporated discontinuous/continuous Ag thin films having mass thicknesses of ~5 and ~10 nm, followed by an annealing at 300 °C for 1 h in nitrogen ambient; these samples are called as C5/ARC5 and C10/ARC10, respectively. Surface morphological studies of Ag NPs were carried out using Carl Zeiss scanning electron microscope (SEM). The Ag NPs were also prepared on glass substrates with the similar experimental conditions for transmittance measurements.

Total transmission (TT) and total reflectance (TR) measurements were performed using Perkin Elmer Lambda 1050 double beam UV–Vis–NIR spectrophotometer having 150 mm integrating sphere as an attachment. The current density–voltage (J–V) graphs of cells were carried out under the standard test conditions of the AM1.5G incident light spectra using Oriel Sol3A solar simulator from Newport Corporation, USA. A Keithley 2440 source-meter was used for J–V measurements. External Quantum Efficiency and TR spectra were recorded using SpeQuest quantum efficiency measurement system having an integrating sphere as an attachment from ReRa Solutions, The Netherlands. For IS measurements, Zahner Zennium model potentiostat equipped with frequency response analyser was used. Impedance spectra were recorded from 1 Hz to 1 MHz frequency range with perturbation voltage of 10 mV, and by applying 0.6 V forward DC bias voltage under AM1.5G light illumination from a solar simulator. The IS measurements were carried out on the same cell before (C0/ARC0) and after Ag NPs integration (C5/ARC5 and C10/ARC10), in order to avoid area dependent variations during measurements. The obtained impedance semicircles were fitted using ZView program, with different combinations of inductor, resistor, and capacitor in an equivalent circuit model. All the characterization experiments were conducted at room temperature.

3. Results and discussion

The SEM micrographs of the Ag NPs prepared on textured silicon cells without ARC (C5 and C10) and with ARC (ARC5 and ARC10) are presented in Fig. 1. Relatively larger size NPs formation can be seen in the case of cell C10 when compared to on cell C5, which is due to the large initial Ag film mass thickness. There is no considerable variation in the size or surface coverage of Ag NPs when prepared on the Si_3N_4 layer coated textured silicon surface. Due to large surface coverage of NPs, it appears like 2-dimensional Ag NPs layer.

The J–V measurements for cells without (C0) and with the Ag NPs (C5 and C10) are presented in Fig. 2a, the inset table shows the photovoltaic parameters of corresponding cells. From Fig. 2a, it is apparent that the cell efficiency is slightly decreased after the Ag NPs integration. The decreasing trend in current density and efficiency of cells after Ag NPs integration is also presented in Fig. 2c in the form of standard box plot. This represents distribution of current density and efficiency values of three cells corresponds to Ag film thickness of ~5 and 10 nm. Internal quantum efficiency (IQE) and TR spectra of cells C0, C5 and C10 are presented in Fig. 2b, from which one can

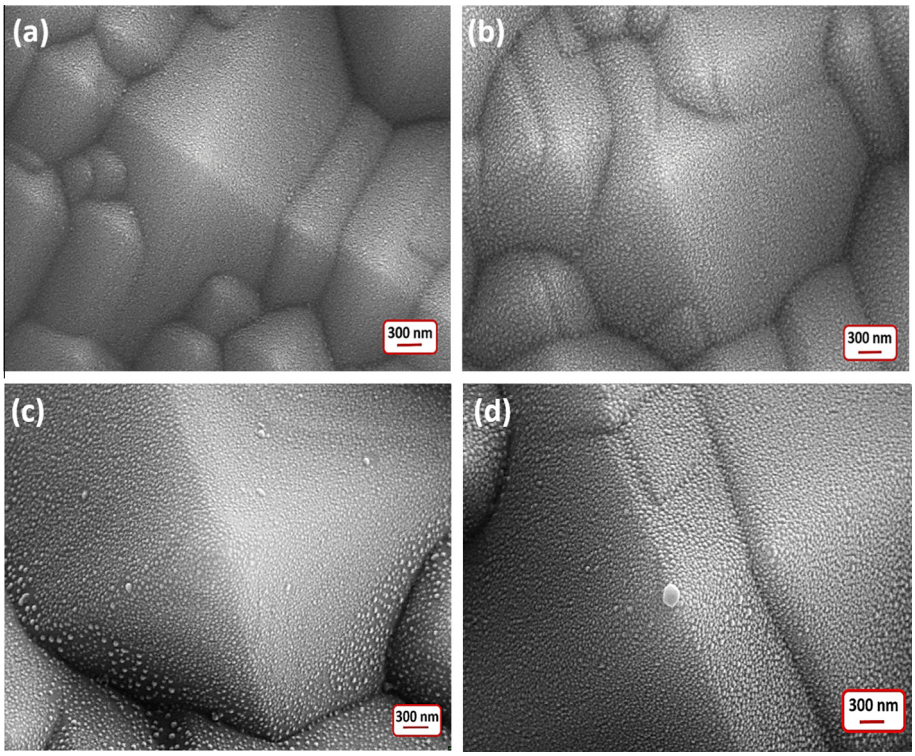

Fig. 1. SEM micrographs of silver nanoparticles prepared on textured silicon solar cells without (a and b) and with (c and d) the ~75 nm Si_3N_4 layer from ~5 nm (a and c), and ~10 nm (b and d) thin silver films after annealing at 300 °C.

observe an incident photon to current conversion efficiency modification with different sizes of the Ag NPs on the textured silicon surface. In the IQE spectra, the significant reduction in photocurrent near the SPR region of the Ag NPs is observed as compared to the off-resonant region. A peak in the TR spectra around ~500 nm is due to back scattering from relatively larger sized NPs of C10 as compared to C5. If the losses are associated only with increased reflectance from the Ag NPs, these should not reflect in the IQE spectra, since it takes into account the reflection losses from the Ag NPs. Therefore, the reduced IQE near the SPR region could be due to parasitic absorption losses from the Ag NPs and modified charge carrier recombination at cell emitter-Ag NPs interface. The latter phenomenon is often overlooked due to dominance of the parasitic absorption losses from the Ag NPs. Further understanding is essential to gain more insights related to the Ag NPs influence on plasmonic cell electronic performance.

One of the ways to quantify the parasitic absorption losses from the Ag NPs is measuring of absorptance spectra. We estimated absoprtance (A) from experimentally measured TT and TR spectra using the relation; A = 1–TT–TR (Morawiec et al., 2013). The absorptance spectra of NPs on glass substrates are presented in Fig. 3, from which it is apparent that the parasitic absorption losses are significant near the SPR region of Ag NPs. With a slight increase in the NPs size (see SEM images in Fig. 1b and d), the broadening in spectra is observed with a small shoulder at short wavelengths region, which is an indication of relatively large NPs formation with the increase in Ag film thickness. With this observation, one can infer that reduced IQE of C10 than C5 cells near the SPR region is to some extent from the parasitic absorption losses. Our observations contradicting to the earlier report (Evanoff and Chumanov, 2004) that the parasitic absorption losses are more in small Ag NPs as compared to large NPs. The proportionate increase of absorption with size in our case could be due to the polycrystalline nature of Ag NPs (Santbergen et al., 2012). Although the NPs size on glass substrate and silicon surface may not be identical at a given annealing temperature (due to thermal conductivity and surface morphology variations), but the absorptance spectra give an idea about losses related to Ag NPs on a silicon cell.

The presence of thin dielectric spacer layer between the cell and Ag NPs may segregate the parasitic absorption losses and interfacial charge carrier recombination by providing electronic separation. With this motivation, the Ag NPs are also prepared on cells coated with ~75 nm Si_3N_4 ARC layer under similar conditions. After the Ag NPs integration on the Si_3N_4 coated cell, a gradually decrease in J_{sc} is also observed with increase in Ag NPs size (J–V graphs not shown here) in similar to cells without Si_3N_4 layer. The IQE and TR spectra of Ag NPs integrated on ARC coated cells are presented in Fig. 4. Apart from some increase in reflectance near the SPR region, rest of the TR spectra are almost unaffected by the Ag NPs integration. In similar to cells without a Si_3N_4 layer, the IQE is also reduced near the SPR region ($\lambda \sim 430$ nm) in cells with

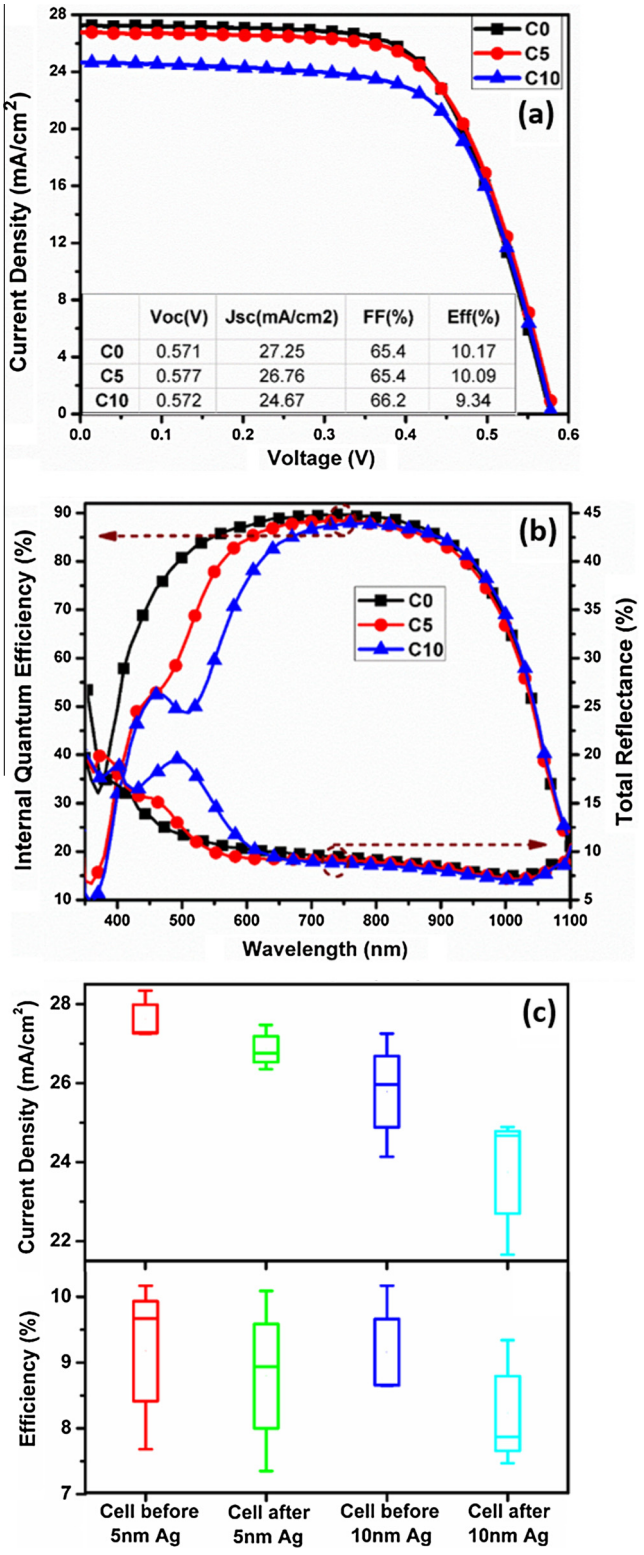

Fig. 2. (a) Current density–voltage graphs of bare cell C0, and silver nanoparticles integrated cells C5 and C10. Inset table of Fig. (a) shows the photovoltaic parameters of cells C0, C5 and C10. (b) Internal quantum efficiency and total reflectance spectra of silver nanoparticles integrated cells C5, C10 and bare cell C0. (c) The distribution of current density and efficiency values of three silicon cells without and with silver nanoparticles (prepared from ~5 and 10 nm silver films) represented in a box plot form.

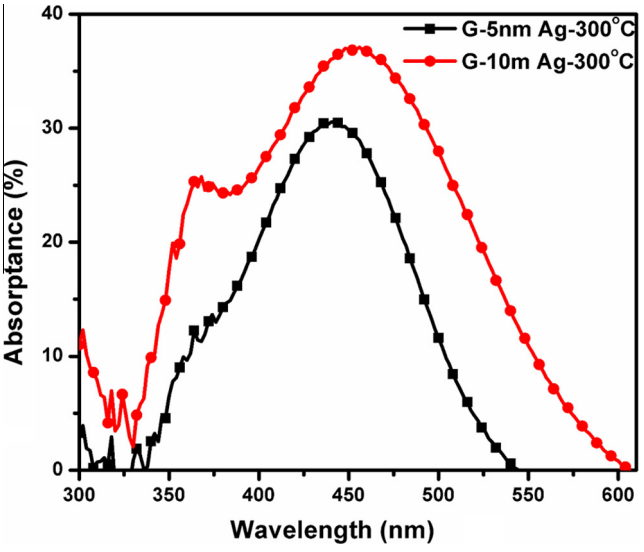

Fig. 3. Absorptance spectra of silver nanoparticles prepared on glass substrates from annealing silver films of thickness ~5 nm and ~10 nm at 300 °C.

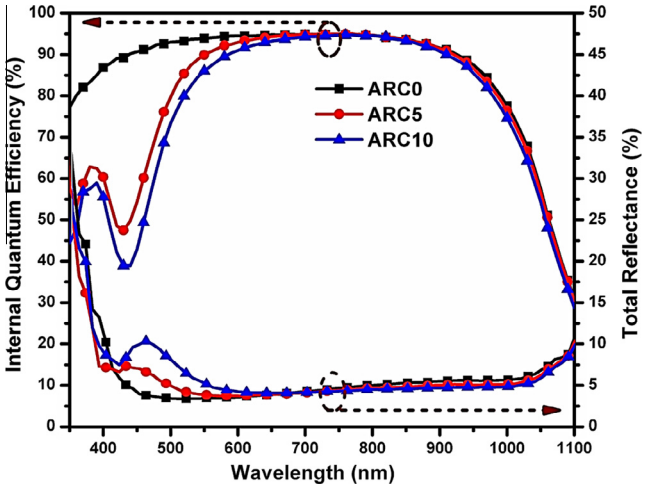

Fig. 4. Internal quantum efficiency and total reflectance spectra of silver nanoparticles integrated on cells ARC5, ARC10, and bare cell ARC0.

Si_3N_4 layer. From these observations, we can infer that the reduced IQE near the SPR region is due to the parasitic absorption from the Ag NPs only, with the assumption that Si_3N_4 spacer layer minimizes the interfacial recombination losses from the Ag NPs' intense near-fields. A similar type of decrement in quantum efficiency due to the parasitic absorption from metal NPs was also reported from a variety of plasmonic solar cells (Hylton et al., 2013; Daif et al., 2012). A few changes are noticed after comparing Figs. 2b and 4, which are; a sharp valley in the IQE spectra of ARC5 cell whereas it is broad in the case of C5 cell, and a blue shift in the SPR valley position of ARC10 cell as compared to C10. These changes are primarily due to the modified dielectric environment for the

Ag NPs' SPRs. The Ag NPs on Si_3N_4 coated cell exhibit a blue shift in the SPR wavelength position as compared to Ag NPs on silicon cell, which is due to the variation in restoring force of oscillating free electrons of the Ag NPs.

It is evident from IQE that there is a strong parasitic absorption loss from Ag NPs, however, still it is inconclusive that up to what extent the Ag NPs can influence charge carrier recombination process in plasmonic cell. Since various type of charge carrier dynamics are involved in a solar cell operation, the minority charge carrier lifetime estimation from silicon can provide some details about carrier recombination process. In a recent study, the enhancement in minority carrier lifetimes of plain n-type and p-type silicon wafers is demonstrated after integration of Ag NPs of various sizes and concentration, and the observed phenomenon was explained based on partial field effect passivation from SPR near-fields of Ag NPs (Thouti et al., 2016). In this case, the Ag NPs interaction on the textured silicon solar cell will be different than on the wafer, due to changes in charge carrier dynamics (surface recombination) after texturization of silicon surface as well as with Si_3N_4 ARC layer on front surface.

Hence, the impedance spectroscopy is employed for estimating passive components and thereby τ_{eff} values of plasmonic silicon cell. Impedance spectra (also called as Nyquist plot) is a complex plot between real and imaginary parts of impedance, which can be formulated as represented in Eq. (1). The obtained experimental IS data is fitted using ZView program with an equivalent circuit model (showed as an inset of Fig. 5a). The equivalent circuit model consists of a single parallelly connected resistance–capacitance in series with a resistance, which is represented by the following equation related to device frequency dependant impedance (Kumar et al., 2010).

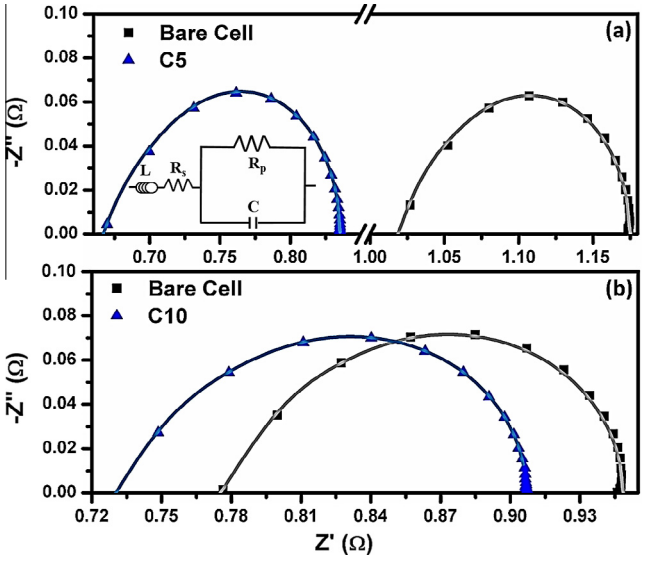

Fig. 5. Under AM1.5G illumination condition, Nyquist plots of cells (a) C5 and (b) C10 before and after silver nanoparticles integration with 0.6 V forward bias voltage (symbols represent experimental data points and lines represent fitted curves using proposed model).

$$Z^*(\omega) = R_s + \frac{R_p}{1+(\omega R_p C_p)^2} - j\frac{\omega C_p R_p^2}{1+(\omega R_p C_p)^2} \quad (1)$$

where ω is frequency of applied signal, R_s, R_p and C_p are series resistance, parallel resistance and parallel capacitance, respectively.

The primary and secondary intercepts of Nyquist plot on Z' (horizontal) axis from the origin correspond to R_s and $R_s + R_P$, respectively. The passive component values (i.e., R_s, R_P, and C_p) are obtained by the fitting of experimental IS semicircles by adopting proposed equivalent circuit model. The R_s represents series resistance of cell along with connecting leads, R_p represents recombination resistance, and C_p parallel capacitance of proposed device. The R_p and C_p are manifestations of cell junction properties. At reverse and low forward bias conditions, the C_p is dominated by depletion capacitance (C_{dl}), and at sufficiently large forward bias voltage (open-circuit voltage of cell) C_p is dominated by diffusion capacitance (C_μ) or also called chemical capacitance (Sero et al., 2009). The C_μ also represents any modification in carrier density (variation of the Fermi level position), like an increase in minority carrier density when device is in forward bias condition. The estimated R_p and C_p values are further used for calculating the τ_{eff} ($=R_p \times C_p$).

The Nyquist plots of cells C0, C5 and C10 with 0.6 V forward bias voltage and under AM1.5G illumination (100 mW/cm^2) are presented in Fig. 5. The comparison we made with 0.6 V bias voltage which is slightly greater than the open circuit voltage of all cells. In this condition, the excess carrier concentration will be homogeneous in base-emitter region, so, the capacitance will be governed by diffusion of charge carriers that are being generated outside the depletion region, from which the τ_{eff} values are estimated. The inductor element is also included in the equivalent circuit model for fitting Nyquist plots (inset of Fig. 5a), because the connecting leads show some inductance behavior with high frequency applied bias voltage.

The Nyquist plots of ARC coated cells before and after the Ag NPs integration are presented in Fig. 6. The horizontal shift of Nyquist plots toward right side indicates an increase in R_s with Ag NPs on ARC coated cells, which is opposite to cell without ARC layer (Fig. 5) where the R_s is decreased. Similar change in R_s with the Ag NPs is also observed from J–V measurements (not shown here), an increase in R_s after Ag NPs integration is also reported for ARC coated cells (Park et al., 2013). The decrease in R_s with Ag NPs on without ARC coated cells (Table 1) shows that the NPs are in direct contact with the emitter surface of cell, which can provide an easy path for charge carrier conduction. From J–V measurements, such a similar reduction in R_s after Ag NPs integration is also observed in case of textured cells without ARC coating (Sardana et al., 2014). The passive component values of cells with and without ARC, and also with and without Ag NPs are summarized in Table 1. With the Ag NPs, an increase in diameter of Nyquist plot (Figs. 5 and 6)

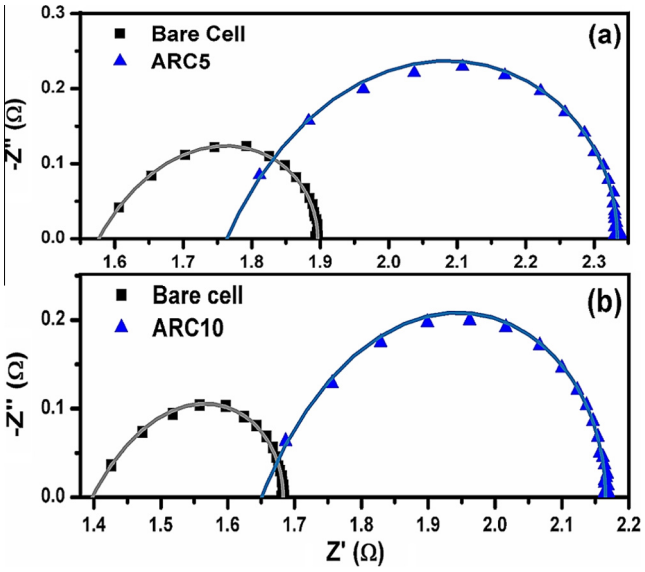

Fig. 6. Under AM1.5G illumination condition, Nyquist plots of cells (a) ARC5 and (b) ARC10 before and after silver nanoparticles integration with 0.6 V forward bias voltage (symbols represent experimental data points and lines represent fitted curves using proposed model).

(without and with ARC) signifies that R_p is increasing and C_p is decreasing due to modification in carrier density generation. Usually the modification of passive components can be expected either any changes in internal structure (modification in interface states and bulk states) or external modification of device. In both cell configurations, the Ag NPs are placed on top of device structure, so, there is no change in the internal structure of device. The parasitic absorption from Ag NPs can decrease the light absorption in cells, leading to decrease in photo-excited charge carriers compared to the reference cell (C0/ARC0).

In general, generated charge carrier concentration is inversely proportional to the resistivity (R_p) of a semiconductor; therefore an increase in R_p is expected due to reduced photocarrier generation after parasitic absorption loss from the Ag NPs. In bare cell without ARC (C0), the front surface recombination is strong due to the absence of surface passivation layer. The decrease in photo-carrier generation near the front surface can also decrease the surface recombination in plasmonic cell as compared to bare cell. In addition to this, the Ag NPs layer can also act as a partial surface passivation layer up to some extent after placing directly on cell emitter surface (without ARC layer) (Thouti et al., 2016). The reduced surface recombination process on cell emitter surface leading to a small decrease in the C_p (from 48.68 to 41.26 μF for cell C5 and from 55.71 to 50.75 μF for cell C10), and further a small decrease in τ_{eff} value. On other hand, in the case of bare cell with ARC (ARC0), the front surface recombination is already minimized with the Si_3N_4 passivation layer, after the Ag NPs integration, the parasitic absorption losses led to a decrease in the photo carrier generation near the front surface. Due to ~75 nm Si_3N_4 spacing from cell, the Ag NPs cannot act as a partial surface passivation layer as compared to cell without Si_3N_4. So, the strong parasitic absorption losses only led to substantial decrease in C_p (from 40.66 to 21.28 μF for cell ARC5, and from 38.65 to 22.11 μF for cell ARC10) with reduced photo-carrier generation, resulting in a large decrease in τ_{eff} values.

From the obtained passive components of all cells, the τ_{eff} values are estimated and listed in Table 1. The τ_{eff} values of cells C5 and C10 are decreased from 9.93 to 9.57 μs and from 12.03 to 11.77 μs, respectively, the decrease in τ_{eff} is very small and which may not support the observed decrease in photocurrent from *J–V* and IQE measurements. However, in case of cells ARC5 and ARC10 the τ_{eff} values are considerably decreased from 17.76 to 15.04 μs and from 16.07 to 14.57 μs, respectively. For cells without ARC, the parasitic absorption losses and surface passivation by Ag NPs may compete, and result in a small decrease in τ_{eff} values. On the other hand, in ARC coated cells, the only loss mechanism is parasitic absorption losses from Ag NPs which led to a large decrease in τ_{eff}. We observed a strong modification in the C_p with reduced light transmission into a cell structure; Kumar et al. (2014) also observed modified C_p with illumination intensity, whereas Sero et al. (2009) observed no change in C_p with the illumination intensity. The available information from the literature on impedance spectroscopy studies of silicon solar cells is discrete and also inadequate to draw a major

Table 1
Estimated passive component values and effective minority carrier lifetime values of solar cells before (C0/ARC0) and after Ag NPs integration (C5/C10/ARC5/ARC10). The values are obtained by fitting experimental impedance spectra recorded at 0.6 V forward bias voltage under AM1.5G illumination conditions (values within brackets show the percentage of error in fitting).

	Bare silicon solar cell (C0/ARC0)				Silicon solar cell with Ag nanoparticles			
	R_s (Ω)	R_p (Ω)	C_p (μF)	τ_{eff} (μs)	R_s (Ω)	R_p (Ω)	C_p (μF)	τ_{eff} (μs)
C5	0.97 [±0.09]	0.204 [±0.43]	48.68 [±0.96]	9.93	0.602 [±0.1]	0.232 [±0.27]	41.26 [±0.61]	9.57
C10	0.732 [±0.08]	0.216 [±0.28]	55.71 [±0.67]	12.03	0.674 [±0.1]	0.232 [±0.28]	50.75 [±0.63]	11.77
ARC5	1.459 [±0.11]	0.437 [±0.37]	40.66 [±0.77]	17.76	1.626 [±0.19]	0.707 [±0.44]	21.28 [±0.98]	15.04
ARC10	1.266 [±0.15]	0.416 [±0.46]	38.65 [±0.92]	16.07	1.506 [±0.19]	0.659 [±0.44]	22.11 [±0.96]	14.57

conclusion. Therefore, further detailed experiments may require to understand the recombination kinetics in plasmonic solar cells. Our experimental results are explained by considering that there is no influence of annealing step on passive components. Although, the cells were pre-annealed for excluding annealing related modifications, re-annealing of cell for obtaining NPs may also have some influence on the passive components of device.

4. Conclusions

The quantum efficiency measurements of plasmonic textured silicon cells without and with Si_3N_4 spacer layer revealed that the Ag NP layers act adversely on cell performance due to the parasitic absorption losses near the SPR region. Using impedance spectroscopy, we estimated passive components of cells like; series resistance, recombination resistance, and chemical capacitance after fitting experimentally obtained impedance semi-circles. The Ag NPs on cells without Si_3N_4 spacer layer exhibited a small decrease in τ_{eff} due to surface field effect passivation by NPs. The Ag NPs on the cell with Si_3N_4 spacer layer exhibited a large decrease in τ_{eff} due to the parasitic absorption losses. The parasitic absorption losses from Ag NPs influenced the passive components by suppressing light transmission into the plasmonic cell, which led to a decrease in τ_{eff}. Our observations and understanding may provide some useful information related to any other plasmonics based opto-electronic devices.

Acknowledgements

Authors thank nanoscale research facility of Indian Institute of Technology Delhi for impedance spectroscopy measurements. Authors acknowledge for fruitful discussion with Dr. Sanjai Kumar (Central Electronics Limited, Sahibabad), Mr. Shubham Bansal and Dr. Nikhil Chander (Centre for Energy Studies, IIT Delhi).

References

Atwater, H.A., Polman, A., 2010. Plasmonics for improved photovoltaic devices. Nat. Mater. 9, 205–213.

Barugkin, C., Wan, Y., Macdonald, D., Catchpole, K.R., 2013. Evaluating plasmonic light trapping with photoluminescence. IEEE J. Photovoltaics 3, 1292–1297.

Beck, F.J., Polman, A., Catchpole, K.R., 2009. Tunable light trapping for solar cells using localized surface plasmons. J. Appl. Phys. 105, 114310.

Daif, O.E., Tong, L., Figeys, B., Nieuwenhuysen, K.V., Dmitriev, A., Dorpe, P.V., Gordon, I., Dross, F., 2012. Front side plasmonic effect on thin silicon epitaxial solar cells. Sol. Energy Mater. Sol. Cells 104, 58–63.

Das, S., Kundu, A., Saha, H., Datta, S.K., 2015. Investigating the potential of nanoplasmonics for efficiency enhancement of wafer based crystalline silicon solar cells. Plasmonics 10, 1895–1907.

Evanoff Jr., D. David, Chumanov, George, 2004. Size-controlled synthesis of nanoparticles. 2. Measurement of extinction, scattering, and absorption cross sections. J. Phys. Chem. B 108, 13957–13962.

Hylton, N.P., Li, X.F., Giannini, V., Lee, K.H., Ekins-Daukes, N.J., Loo, J., Vercruysse, D., Van Dorpe, P., Sodabanlu, H., Sugiyama, M., Maier, S.A., 2013. Losses mitigation in plasmonic solar cells: aluminium nanoparticles for broadband photocurrent enhancement in GaAs photodiodes. Sci. Rep. 3, 2874.

Kumar, S., Singh, P.K., Dhariwal, S.R., 2010. Effect of surface passivation on generation and recombination lifetimes in silicon wafer studied by impedance spectroscopy. Appl. Phys. Lett. 96, 162109.

Kumar, S., Vandana, Rauthan, C.M.S., Kaul, V.K., Singh, S.N., Singh, P. K., 2014. Spectral and injection level dependence of recombination lifetimes in silicon measured by impedance spectroscopy. IEEE J. Photovoltaics 4 (1), 380–386.

Manisha, S., Pudasaini, P.R., Francisco, R.Z., Katerina, V., Arturo, A.A., 2014a. Plasmonic effects of Au/Ag bimetallic multi spiked nanoparticles for photovoltaic applications. ACS Appl. Mater. Interfaces 6, 15472–15479.

Manisha, S., Pudasaini, P.R., Francisco, R.Z., David, E., Arturo, A.A., 2014b. Ultrathin, flexible organic-inorganic hybrid solar cells based on silicon nanowires and PEDOT: PSS. ACS Appl. Mater. Interfaces 6, 4356–4363.

Morawiec, S., Mendes, M.J., Mirabella, S., Simone, F., Priolo, F., Crupi, I., 2013. Self-assembled silver nanoparticles for plasmon-enhanced solar cell back reflectors: correlation between structural and optical properties. Nanotechnology 24, 26501–26512.

Park, J., Rao, J., Kim, T., Varlamov, S., 2013. Highest efficiency plasmonic polycrystalline silicon thin film solar cells by optimization of plasmonic nanoparticle fabrication. Plasmonics 8, 1209–1219.

Pillai, S., Catchpole, K.R., Trupke, T., Green, M.A., 2007. Surface plasmon enhanced silicon solar cells. J. Appl. Phys. 101, 093105.

Pudasaini, P.R., Arturo, A.A., 2013. Nanostructured plasmonics silicon solar cells. Microelectron. Eng. 110, 126–131.

Santbergen, R., Temple, T.L., Liang, R., Smets, A.H.M., van Swaaij, R. A.C.M.M., Zeman, M., 2012. Application of plasmonic silver island films in thin-film silicon solar cells. J. Opt. 14, 024010.

Sardana, S.K., Chava, V.S.N., Thouti, E., Chander, N., Kumar, S., Reddy, S.R., Komarala, V.K., 2014. Influence of surface plasmon resonances of silver nanoparticles on optical and electrical properties of textured silicon solar cell. Appl. Phys. Lett. 104, 073903.

Sero, I.M., Belmonte, G.G., Boix, P.P., Vazquez, M.A., Bisquert, J., 2009. Impedance spectroscopy characterization of highly efficient silicon solar cells under different light illumination intensities. Energy Environ. Sci. 2, 678.

Spinelli, P., Polman, A., 2012. Prospects of near-field plasmonic absorption enhancement in semiconductor materials using embedded Ag nanoparticles. Opt. Express 20 (S5), A641.

Spinelli, P., Ferry, V.E., van de Groep, J., van Lare, M., Verschuuren, M. A., Schropp, R.E.I., Atwater, H.A., Polman, A., 2012. Plasmonic light trapping in thin-film Si solar cells. J. Opt. 14, 024002.

Tan, H., Santbergen, R., Smets, A.H.M., Zeman, M., 2012. Plasmonic light trapping in thin film silicon solar cells with improved self-assembled silver nanoparticles. Nano Lett. 12, 4070–4076.

Thouti, E., Sharma, A.K., Sardana, S.K., Komarala, V.K., 2014. Internal quantum efficiency analysis of plasmonic textured silicon solar cells: surface plasmon resonance and off-resonance effects. J. Phys. D: Appl. Phys. 47, 425101.

Thouti, E., Kumar, S., Komarala, V.K., 2016. Enhancement of minority carrier lifetimes in n- and p-type silicon wafers using silver nanoparticle layers. J. Phys. D: Appl. Phys. 49, 015302.

Tong, C., Yun, J., Song, H., Gan, Q., Anderson, W.A., 2014. Plasmonic-enhanced Si Schottky barrier solar cells. Sol. Energy Mater. Sol. Cells 120 (Part B), 591.

Yang, Y., Pillai, S., Mehrvarz, H., Kampwerth, H., Ho-Baillie, A., Green, M.A., 2012. Enhanced light trapping for high efficiency crystalline solar cells by the application of rear surface plasmons. Sol. Energy Mater. Sol. Cells 101, 217.